Point defects in bcc crystals: Structures, transition kinetics, and melting implications

Frank H. Stillinger and Thomas A. Weber
AT&T Bell Laboratories, Murray Hill, New Jersey 07974

(Received 9 July 1984; accepted 2 August 1984)

Structures corresponding to various potential energy minima have been examined for a classical model whose pair interactions produce a body-centered-cubic crystalline ground state. The method used is molecular dynamics computer simulation for 128 particles with frequent steepest-descent mapping onto nearby minima. The elementary structural excitation out of the crystalline absolute minimum is creation of a vacancy, split-interstitial defect pair. This excitation process upon repetition shows a defect softening of the medium. Transition states (saddle points) have been located for some pairs of neighboring minima, and vibrational modes have been calculated for minima and for transition states. A simple melting theory based on these observations is proposed which satisfactorily describes the model's first-order melting behavior.

I. INTRODUCTION

Locating, enumerating, and classifying potential energy minima in many-body systems proves to be a valuable technique for understanding condensed-phase properties. In combination with standard molecular dynamics simulation of classical systems this approach has been applied both to monatomic substances[1–3] and to polyatomic molecular media.[4] It has produced valuable insights concerning the nature of short-range order in liquids and the behavior of amorphous solids.[2]

The preceding paper[5] introduces a specific many-body system for which the low-temperature stable structure is a bcc crystal. In this respect it behaves qualitatively like many of the elements, most notably the alkali metals.[6] The major focus of that paper was study of the pair distribution function and its behavior under the mapping that locates relevant potential energy minima. The present paper reconsiders the same model. The objective now is (i) a more complete characterization of the mechanically stable particle packings (potential energy minima); (ii) a study of saddle points connecting pairs of those minima; and (iii) an application of the information thus achieved to a rudimentary theory of the first-order melting transition in the model.

The general approach of mapping onto local potential minima and details of the specific model used is outlined in the next Sec. II. Section III concentrates on the band of lowest-lying configurational excitations identified for this system, namely that produced by creation of a vacancy, split-interstitial defect pair in the perfect bcc structure. Section IV discusses the identification and analysis of transition states (potential energy saddle points) that connect pairs of potential minima, a topic obviously central to understanding kinetic properties. That insertion of defects into an initially crystalline medium causes "softening," thereby easing further defect insertions, is established in Sec. V. The various properties identified are then assembled in Sec. VI into a melting theory analogous (but not entirely isomorphous) to one proposed earlier for melting in the *two-dimensional* Gaussian core model.[1] Conclusions are summarized in the final Sec. VII.

II. MAPPING AND MODEL

Let $\mathbf{r}$ denote the $3N$-dimensional configuration-space vector for a set of mutually interacting point particles. The potential energy function $\Phi(\mathbf{r})$ generates a natural mapping of the continuum set of $\mathbf{r}$'s onto a discrete set of configurations $\mathbf{R}_\alpha (\alpha = 1,\cdots,\Omega)$ which are the local minima of Φ. Specifically this mapping is constructed by means of the steepest-descent equation

$$\partial \mathbf{r}/\partial s = -\nabla \Phi(\mathbf{r}) \tag{2.1}$$

with the given $\mathbf{r}$ as an initial condition ($s = 0$). The resulting solution $\mathbf{r}(s)$ to Eq. (2.1) will have the property

$$\lim_{s \to +\infty} \mathbf{r}(s) = \mathbf{R}_\alpha \tag{2.2}$$

for some α determined by the initial condition; this defines a mapping

$$\mathrm{M}[\mathbf{r}(0)] = \alpha. \tag{2.3}$$

By this means the full $3N$-dimensional configuration space is divided exhaustively into connected nonoverlapping regions, each of which contains precisely one $\mathbf{R}_\alpha$. Because the $\mathbf{R}_\alpha$ are Φ minima they correspond to mechanically stable arrangements of the N particles. Deviations from the fiducial set $\{\mathbf{R}_\alpha\}$ constitute (generally anharmonic) vibrations. Hence the mapping M effects a separation of the many-body problem into a purely geometric packing part (identification of the $\mathbf{R}_\alpha$) and a vibrational part (displacement from $\mathbf{R}_\alpha$ within the surrounding connected region).

The preceding paper introduced and examined several features of a model in which Φ was pairwise additive:

$$\Phi(\mathbf{r}) = \sum_{i<j=1}^{N} v(r_{ij}), \tag{2.4}$$

where the specific form of v is

$$\begin{aligned} v(r) &= A\,(r^{-6} - r)\exp[(r-a)^{-1}] \quad (0<r<a), \\ &= 0 \qquad\qquad\qquad\qquad\quad (a \leqslant r), \end{aligned} \tag{2.5}$$

with

$$A = 3.809\,745\,436, \quad a = 2.0. \tag{2.6}$$

This central pair potential has depth -1 and passes through

 0021-9606/84/235095-09$02.10

zero when r is $+1$.

As in the preceding paper we shall be concerned with a system of $N = 128$ particles in a cubic cell, subject to periodic boundary conditions. This number of particles can form a perfect body-centered cubic (bcc) array in the given cell, meshing perfectly with its periodic images. The reduced density $\rho^* = 0.730\,51$ is that which minimizes the lattice energy at the value

$$\Phi = -841.985\,87,\ \Phi/N = -6.578\,015 \quad \text{(perfect bcc)}. \tag{2.7}$$

The reduced melting and freezing temperatures at this density (which we continue to employ below) are

$$T_m^*,\ T_f^* \cong 0.43 \tag{2.8}$$

By carrying out the mapping Eqs. (2.1)–(2.3) at frequent regularly spaced intervals during the course of molecular dynamics numerical simulation, it is possible to establish which portions of the configuration space dominate the system's statistical properties. At low energy (low temperature crystal) the mapping places the system at one of the permutation-equivalent absolute minima as expected. When the conserved total energy is high, by contrast, the mapping typically yields a rapidly changing sequence of $\mathbf{R}_\alpha$'s that predominantly corrospond to amorphous random packings. These latter are the inherent structures which underline the stable liquid phase.

The mapping onto potential energy minima produces particularly vivid and informative patterns while the system is undergoing a phase transition. Figure 1 provides an excellent example, wherein values of

$$\Phi = \Phi(\mathbf{R}_\alpha)/N, \tag{2.9}$$

the potential per particle at the relevant minima, are given

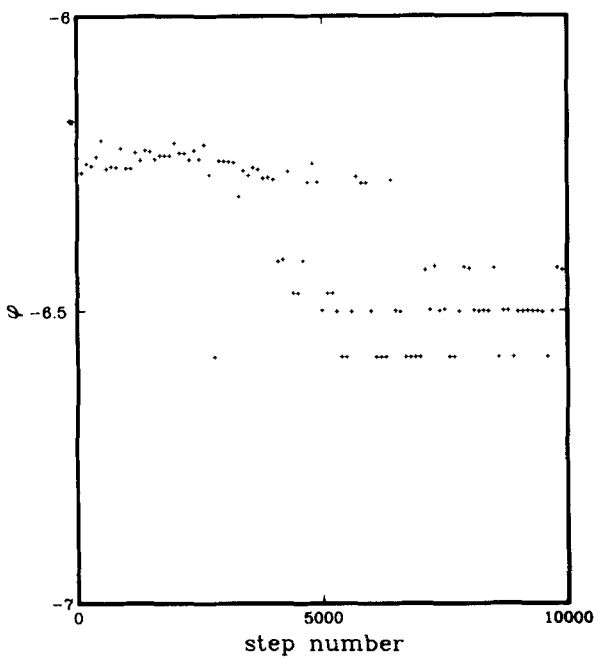

FIG. 1. Potential energy per particle (ϕ) at minima located by steepest-descent mapping during the course of a molecular dynamics run. Mapping is carried out every 100 time steps (i.e., every 0.125 time units). The system initially was a supercooled liquid at reduced temperature 0.34. Nucleation of the bcc crystal phase begins after about 4000 steps have elapsed.

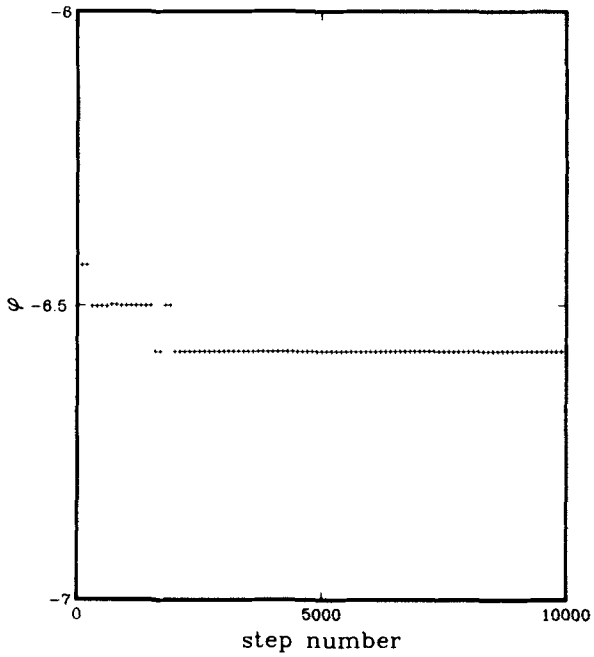

FIG. 2. Potential energy per particle (ϕ) at minima located by steepest-descent mapping during extension of the sequence shown in Fig. 1. The result on every occasion after step 2000 is the absolute minimum, indicating that the 128-particle system resides near a perfect bcc crystalline arrangement.

every $\Delta t = 0.125$ (every 100 time steps) for a sequence during which freezing spontaneously initiated in a slightly supercooled liquid. At first (up to about step number 4000) the mapping sampled primarily the high-Φ manifold of amorphous states previously identified for this system.[5] Subsequently a set of low Φ values appeared, with a nonuniform distribution exhibiting substantial banding. Figure 2 shows the extension of the same dynamical sequence. Only the absolute minium Φ value given in Eq. (2.7) emerges from the

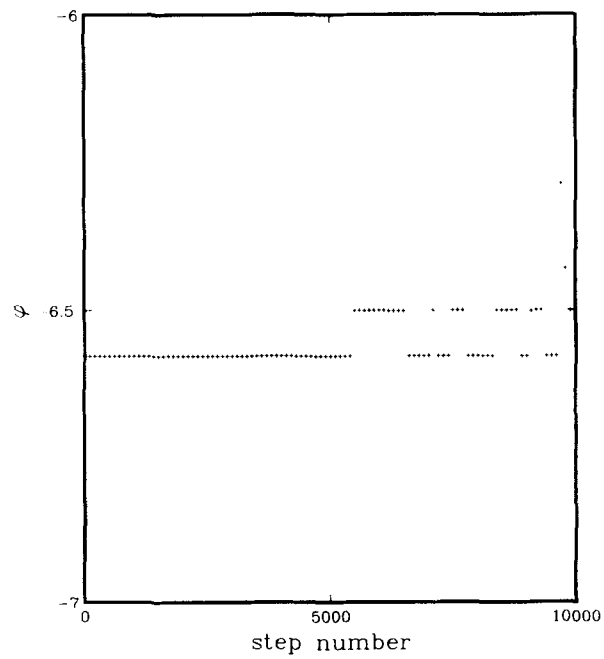

FIG. 3. Sequence of local minima in potential energy (on a per particle basis) resulting from steepest-descent mapping during melting of the bcc crystal. The initial reduced temperature is 0.50.

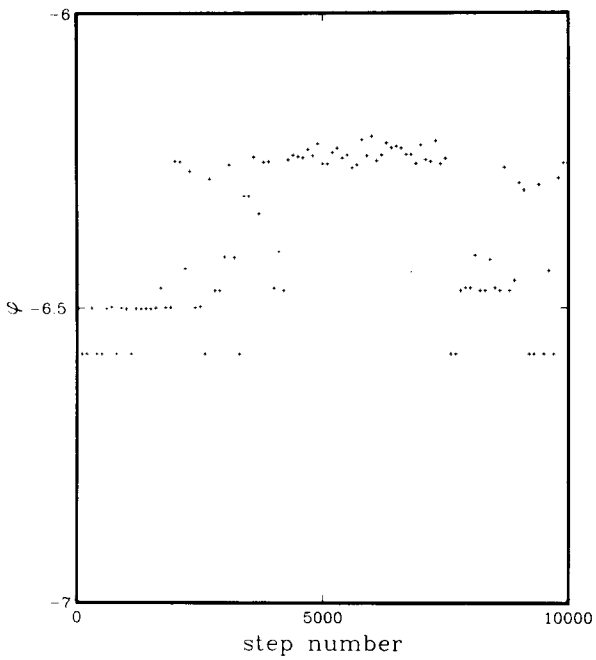

FIG. 4. Continuation of the mapping sequence for the melting event in Fig. 3.

mapping after 2000 time steps indicating that freezing was complete.

Figures 3–5 display Φ values for the mapping during the inverse process, namely melting of the perfect bcc crystal. Once again the system is observed to traverse a portion of its multidimensional configuration space that has bands of relatively low-lying potential energy minima.

III. FIRST EXCITATION BAND

The narrow and isolated band of states seen in Figs. 1–4 near $\Phi = 6.50$ are the lowest-lying configurational excitations that have been encountered for the system under investigation. During our extensive numerical studies we have uncovered, all told, 46 distinct Φ values in this band. These are presented in Fig. 6. in "line spectrum" form with an expanded Φ scale to enhance visibility. It should be remarked that most of these stable packings have been encountered many times, often during examination of thermodynamic states at very different temperatures. Although some distinct Φ values in the first excitation band may have been missed, it seems to us likely that most have been observed and recorded.

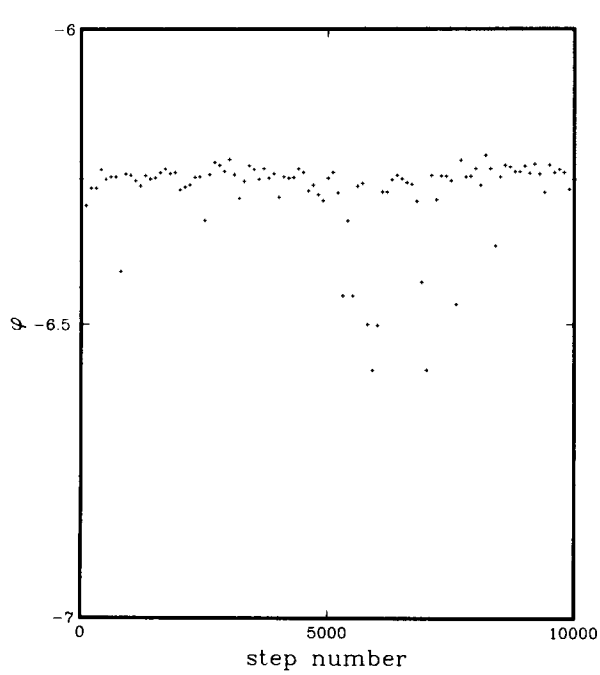

FIG. 5. Continuation of the mapping sequence in Figs. 3 and 4. The final temperature in the liquid is 0.41.

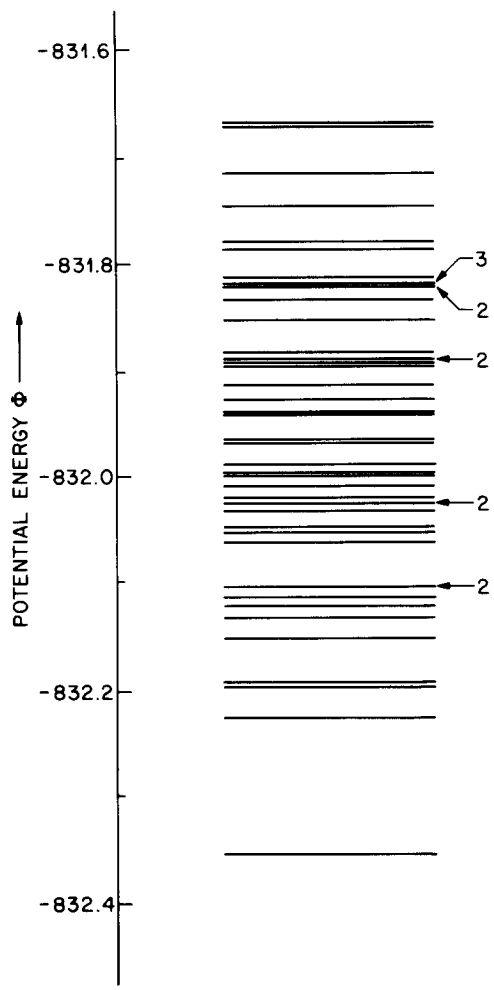

FIG. 6. "Line spectrum" of packing energies (local potential minima) in the first excitation band. In spite of the expanded scale, four pairs and one triplet of distinct energies as indicated remain unresolved graphically.

No obviously simple pattern suggests itself in the packing energies displayed in Fig. 6 that might provide a clue about the nature of these configuration states. However, pictures of the stable packings provide the necessary clarification. Figure 7 gives a set of stereoscopic pairs for three mutually perpendicular views of the lowest-energy packing in this first excitation band. The potential energy of this lowest excited state is

$$\Phi = -832.355\,25. \tag{3.1}$$

Examination of the stereo pictures reveals that this state is a bcc crystal with a close pair of point defects, namely a vacancy and a "split interstitial."[7] The latter consists of two

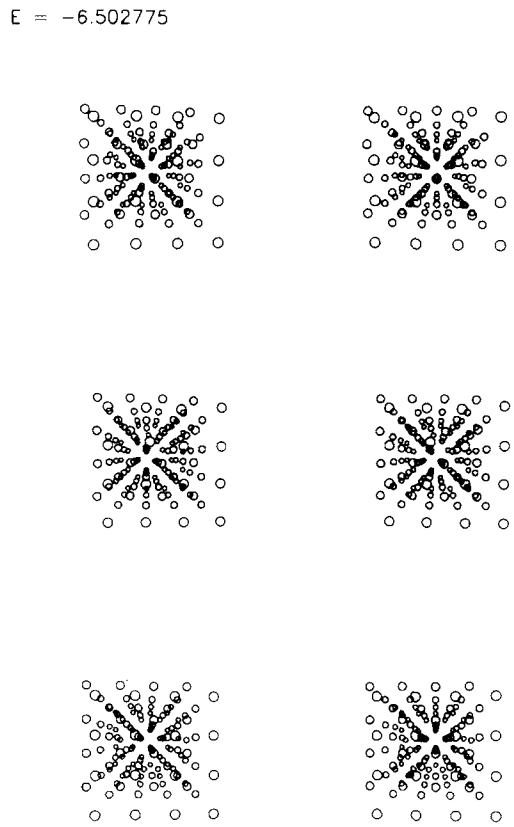

FIG. 7. Stereoscopic picture pairs for the lowest state in the first excitation band.

particles symmetrically disposed about the site where only one should be present in the defect-free crystal. The split interstitial in this instance is oriented parallel to a cube edge; both it and the vacancy lie in the same plane of atoms parallel to a cube face as indicated schematically in Fig. 8.

As a result of their closeness, the vacancy and split interstitial doubtless interact strongly. One effect of this interaction is quite unexpected. Nominally the plane of atoms shown in Fig. 8 would seem to be a reflection symmetry plane, with atoms above and below in symmetric pairs. However that turns out not to be the case upon careful study of the stereo pairs in Fig. 7. Instead, atoms flanking the vacancy in planes directly above and below that containing both defects manifest a spontaneous chiral distortion that destroys the reflection symmetry of the configuration. This chiral distortion can occur in either of two equivalent senses of course and its presence converts what would have been a single potential minimum into two.

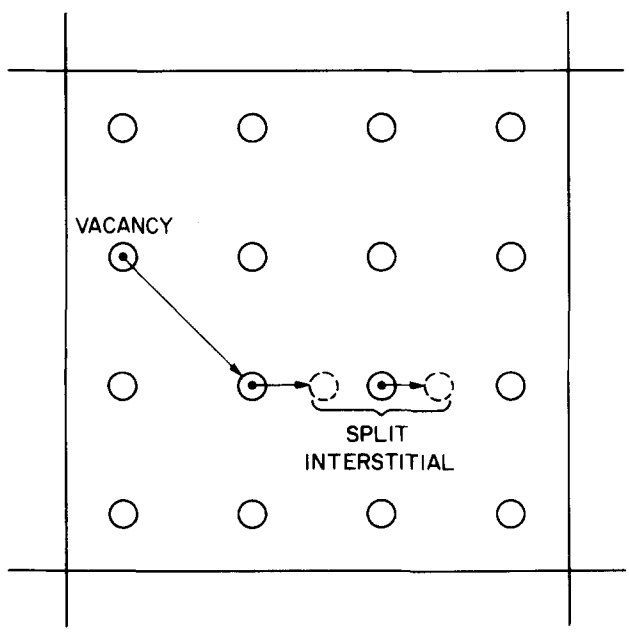

FIG. 8. Schematic diagram showing formation of a coplanar vacancy, split-interstitial defect pair in the lowest state of the first excitation band.

Stereo pictures have also been examined for several other packings selected at random from the first excitation band. They all display a vacancy, split-interstitial pair in an otherwise perfect bcc crystal, however the relative separation of the defects varies from case to case. In particular the configuration shown in Figs. 7 and 8 has the smallest observed separation and this helps to explain the fact that it yields the lowest-energy state in the band. Evidently any smaller separation (see Fig. 8 for instance) would be unstable: The vacancy and split interstitial would have no barrier to prevent spontaneous recombination and annihilation.

The visual sampling of states uncovers two further facts. First, the split interstitial can have a second orientation, namely along a cube diagonal. Second, when the vacancy is farther from the split interstitial than it is in the lowest excited state (Figs. 7 and 8), no perceptible chiral distortion of its flanking particles is observed.

Taking the two orientations of the split interstitial into account, and the fact that the two defects cannot be too close, 46 seems to be a reasonable approximation to the number of distinct packings expected in the first excitation band.

Having thus established that at fixed density the fundamental structural excitation is creation of a vacancy, split-interstitial pair, it is natural to expect another band of excited states to appear at about twice the previous potential energy increment over the ground state, containing two such defect pairs. Indeed such a double excitation band does exist, some components of which are visible in Fig. 1. One of these double-excitation structures, for which

$$\Phi = -823.217\,92, \tag{3.2}$$

is presented as stereo pairs in Fig. 9. The alignment of the crystalline medium with the cubic periodic cell sides (the viewing directions) is still clear.

Perhaps triple-excitation states exist as well, but we have not specifically identified any. They would be expected to occur in a range of Φ overlapping and likely indistinguishable from the large family of more-or-less amorphous packings.[5] Any such band would probably be rather wide in comparison with the single and double excitation bands.

With periodic boundary conditions, particles can pack into largely crystalline arrays that are rotated with respect to the cubic cell edge directions. These rotated configurations fit next to, and are locked into position by, their surrounding periodic images. Figure 10 provides stereo pairs for such a rotated crystal, whose potential energy is

$$\Phi = -827.641\,92 \tag{3.3}$$

That this lies well above the absolute minimum value shown

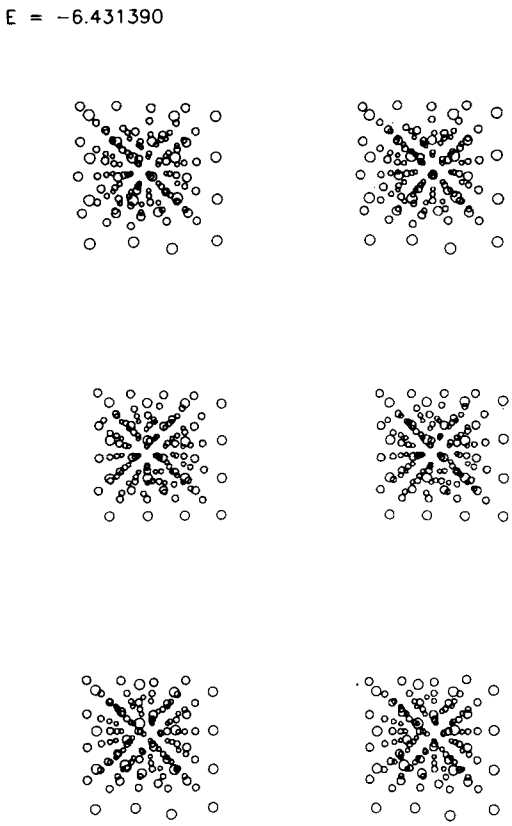

FIG. 9. Stereoscopic picture pairs for a double excitation structure. The potential energy Φ is $-823.217\,92$.

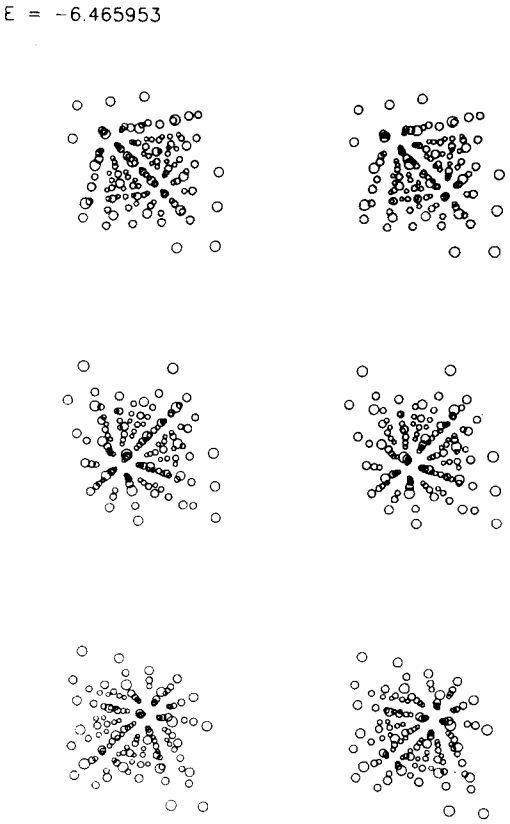

FIG. 10. Stereoscopic picture pairs for a rotated crystal structure. The potential energy Φ is $-827.641\,92$.

in Eq. (2.7) is due to the anisotropic strain that must be present to accommodate the locking onto images. The existence of these rotated crystals and their own excitation bands substantially complicates the task of classifying potential energy minima.

IV. TRANSITION STATES

It is important to identify and characterize "saddle points" on the Φ hypersurface in order fully to understand dynamics of transition between regions surrounding minima. These saddle points are extrema with one or more negative curvatures (imaginary frequencies). Greatest interest perhaps centers about those "simple saddle points" or "transition states" that have just a single negative principal curvature, the direction of which is locally the reaction coordinate direction for the transition. The boundary separating the two regions connected by the reaction coordinate of course must pass through the simple saddle point.

Locating these saddle points is a more demanding task than locating local Φ minima. However, it helps to observe that each saddle point (in addition to each Φ minimum) is a point at which the quantity

$$\Psi = [\nabla \Phi]^2 \tag{4.1}$$

achieves its absolute minimum, namely zero. Therefore the same general types of numerical procedures can be used as before, provided a reasonably close approximation to the saddle point is first in hand. Such an approximation can sometimes be found by the following procedure:

(i) select a pair of Φ minima which the mapping indicates to occur in direct succession during dynamical evolution of the system;

(ii) calculate Φ along a linear path in the $3N$-dimensional space between the two minima;

(iii) identify the configuration along that path, between the minima, at which Φ passes through a maximum. This configuration is then used as a starting point in searching for a nearby Ψ absolute minimum (equal to zero). At times this procedure locks onto local Ψ minima greater that zero, or onto Φ saddle points of higher order.

In this event it is necessary to augment the preceding three steps by the following:

(iv) diagonalize the matrix of second Φ derivatives at the given configuration;

(v) if more than one negative eigenvalue appears, move along the direction of the eigenvector corresponding to the most negative of these to an apparent minimum of Φ.

(vi) rediagonalize. Often this will serve to eliminate one (or more) negative eigenvalues and can be repeated if necessary. Eventually a configuration with just a single negative eigenvalue should be obtained. That configuration is the desired approximation to the saddle point.

Once a transition state has been accurately located, small displacements are made along positive and negative directions for the reaction coordinate (eigenvector for the negative eigenvalue). These displaced confgurations are then subjected to the mapping operation to verify which two minima are indeed connected by the transition state.

Using this strategy we have located a few representative

transition states. Probably the most obvious candidate for examination is the transition state separating the absolute Φ minimum (actually 127! distinct configurations in the presence of periodic boundary conditions) from the lowest level in the first excitation band. This transition state has in fact been produced using steps (i)–(vi) above, followed by minimization of the quantity Ψ in Eq. (4.1). The results for this transition state and its flanking Φ minima are indicated in Fig. 11. We find that the barrier to return from the upper to the lower level is only about 0.51, suggesting that the excited state can decay readily if the system is near its melting point. Indeed we have observed the stable crystal just below T_m^* occasionally to flicker into the first excitation band as a result of thermal fluctuations, but such behavior is transitory. Evidently the rapid formation and annihilation of point defects is an important component of crystal anharmonicity for the model under consideration.

Figure 11 also reports some aspects of the normal mode frequency spectrum for the two minima and the transition state. Vibrational free energy (in the harmonic approximation) is determined by the sum of logarithms of positive frequencies. There are 381 such frequencies for the minima, one fewer at the transition state, and the respective sums are shown in the figure.

The maximum frequency for the perfect crystal is sixfold degenerate. Deforming the system configuration toward and through the transition state causes one of these six modes to split off and rise dramatically in frequency, as indicated in Fig. 11. This isolated mode is localized at the split interstitial, with the two crowded particles vibrating out of phase essentially toward and away from each other.

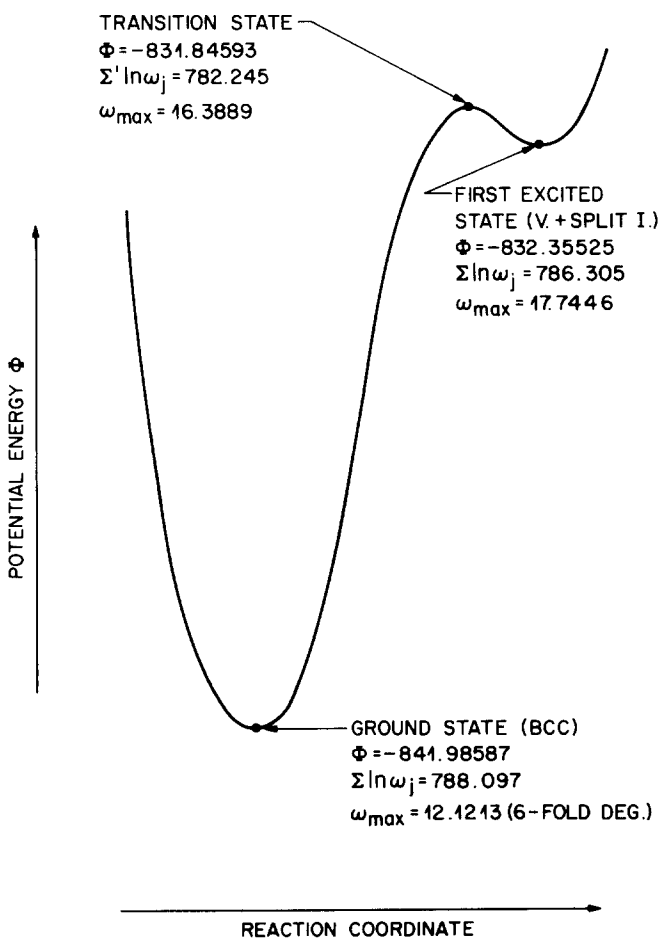

FIG. 11. Characteristics of the absolute Φ minimum, the lowest excitation level, and the transition state between them.

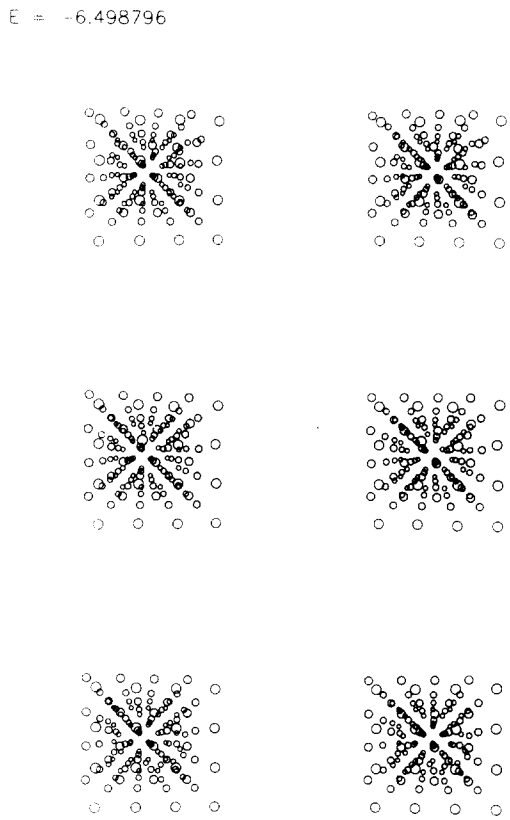

FIG. 12. Stereoscopic picture pairs showing the structure of the transition that appears in Fig. 11.

Figure 12 offers stereo views of the transition state. Consistent with the prior Fig. 8, it requires only a set of displacements localized on a small number of particles to be reached from either minimum.

For the lowest excitation level: (a) there are 128 crystal sites at which the split interstitial could be located; (b) there are three orientations for the split interstitial; (c) there are eight equivalent vacancy sites near the split interstitial; and (d) two chiral distortions are possible about the vacancy. We conclude that each absolute-minimum region possesses

$$128 \times 3 \times 8 \times 2 = 6144 \tag{4.2}$$

equivalent transition states on its bounding hypersurface.

Table I summarizes properties computed for seven transition states (all are simple saddle points). Case A listed there has just been discussed. Cases B and C also involve direct transitions from the absolute minimum to higher levels in the first excitation band. Cases D and E entail transitions *within* the first excitation band, which move the pair of defects around. Cases F and G represent transitions between pairs of minima in the high-Φ amorphous packing group. It is probably no accident that these last two cases have the lowest barriers $\Delta\Phi$ for transition from upper to lower level. This would be expected if the amorphous packing configura-

TABLE I. Transition state properties.

Case	Φ(min)[a]	$\Sigma \ln \omega_j$[b]	Φ(ts)[c]	$\Sigma' \ln \omega_j$[d]	$\Delta\Phi$[e]
A	− 841.985 87	788.097	− 831.845 93	782.245	0.509 32
	− 832.355 25	786.305			
B	− 841.985 87	788.097	− 832.041 34	782.880	0.092 75
	− 832.134 09	786.349			
C	− 841.985 87	788.097	− 831.459 54	780.893	0.574 44
	− 832.033 98	784.111			
D	− 831.915 31	783.447	− 831.276 30	780.757	0.441 61
	− 831.717 91	786.642			
E	− 831.823 55	787.264	− 831.036 85	781.276	0.745 06
	− 831.781 91	783.372			
F	− 796.902 84	756.190	− 796.882 90	753.964	0.019 94
	− 796.911 61	753.924			
G	− 802.250 06	761.102	− 802.201 71	759.600	0.048 35
	− 803.336 54	762.433			

[a] Potential energy of flanking minima.
[b] Vibrational free energy for flanking minima (381 modes).
[c] Potential energy of transition state.
[d] Vibrational free energy of transition state (380 modes).
[e] Barrier to transition from upper to lower minimum.

tions were clustered more closely together in the $3N$-dimensional configuration space than were the low-Φ states.

In each of the cases presented in Table I the reaction coordinates at the transition states entail displacements primarily localized on a small subset of particles. Thus it appears that transition states are not uniformly distributed in all directions about minima in $3N$ space. Instead, they tend to concentrate along directions near small numbers of coordinate axes. This is consistent with our extensive observations on this and other models[2] about overall displacements from minimum to successive minimum during dynamical evolution of the system, namely that these are likewise concentrated on a small subset of the particles.

V. DEFECT SOFTENING

The average increase in potential energy required to elevate the system from its absolute minimum to one of the 46 local minima in the first excitation band is 10.0. Subsequent elevation to the second excitation band for the unrotated crystal appears on average to require somewhat less of an increase, namely 9.4. This reduction can be explained as a mean attraction between point defects. Alternatively it could be described as a defect-softening phenomenon in the crystalline medium, whereby insertion of a few defects makes it easier to insert yet others, at least up to a point. This property had previously been noticed in computations on a two-dimensional system.[1] Furthermore it is consistent with the observation that bulk and shear elastic moduli are less for substances in amorphous compared to crystalline forms.[8]

Defect softening also affects, and is reflected by, the normal modes of vibration at the local Φ minima. To some extent this is illustrated by results listed in Table I. Values of $\Sigma \ln \omega_j$ listed under amorphous-region cases F and G are significantly less than all the others, which pertain to lower-lying (and thus more crystalline) minima. A more complete comparison appears in Fig. 13, which plots $\Sigma \ln \omega_j$ vs Φ for a wide collection of packings. This figure shows the trend just mentioned quite clearly, at least as point defects are inserted into crystals aligned with the box sides (states indicated by solid circles). The same trend is present though less vividly for states identified as misoriented crystals (open circles). In any case fully amorphous states tend to be grouped together with lowest $\Sigma \ln \omega_j$ and highest Φ.

In the large-system limit, boundary conditions should play no role in system properties when examined on a per particle basis. In this respect we believe that the displacement seen in Fig. 13 for the misoriented crystals (that doubtless arises from their substantial anisotropic strain) is a small-system anomaly. The curve drawn in the figure

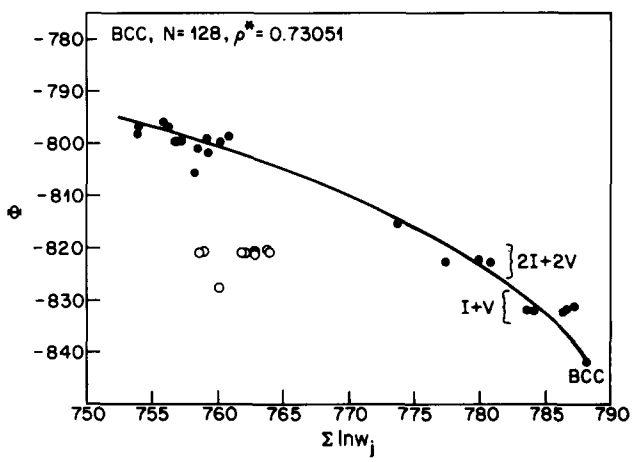

FIG. 13. Plot of potential energy Φ vs vibrational free energy sums $\Sigma \ln\omega_j$ for various packings. Misoriented-crystal cases are shown as open circles.

through the points for properly oriented crystals then is taken to be more indicative of the large-system behavior. Should it become feasible eventually to carry out these calculations on significantly larger systems, and systems with different boundary conditions, this presumption could be checked directly.

The small transition-state barriers $\Delta\Phi$ observed between amorphous state pairs (Table I) compared to those between lower-lying state pairs can also be interpreted as a symptom of defect softening. They indicate that the amorphous medium is relatively easy to rearrange by mechanical means in comparison with the crystal.

VI. SIMPLE MELTING THEORY

Two principal conclusions have thus far emerged, namely that the elementary configurational excitations are vacancy, split-interstitial pairs, and that the medium exhibits defect softening (mean attraction between defects). These ingredients suffice to create a simple melting theory wherein the phase transition is associated with condensation of the gas of defects. The notion that melting should be described by a defect mechanism is hardly new,[9-12] but the specific implementation now to be offered has apparently not appeared in print before. We do not claim universal applicability for the theory, but it seems to be the most appropriate way to describe crystal–liquid transitions in the specific three-dimensional model studied in this paper.

First we note that *any* packing configuration $\mathbf{R}_\alpha$ can formally be described as a bcc crystal containing some number of vacancies and split interstitials. The description is achieved as follows:

(i) Erect a properly oriented bcc reference lattice of N sites within the box, where N is the number of particles in the system. Denote the position of these sites by $\mathbf{s}_i (i = 1,\cdots,N)$;

(ii) connect each particle j in the packing (at $\mathbf{R}_{\alpha j}$) to one of the reference sites, say $\mathbf{s}_{cj}$. This connection c is to be carried out so that no reference site eventually has more than two particles attached to it. Obviously there are many different possible connections which satisfy this restriction;

(iii) calculate the total connection distance $D(c)$ according to the formula

$$D^2(c) = \sum_{j=1}^{N} (\mathbf{R}_{\alpha j} - \mathbf{s}_{cj})^2; \tag{6.1}$$

(iv) minimize $D(c)$ with respect to all permissible connections c and all relative translations of the packing and reference lattice

$$D_0(c_0) = \min D(c). \tag{6.2}$$

The minimizing connection scheme c_0 assigns 0, 1, or 2 particles (respectively, vacancies, single particles, split interstitials) to each bcc site, thereby formally accomplishing the classification task.

Against this background we can now produce an approximate canonical partition function Z_N for the model system. This will be done in two easy stages. The first incorporates defects but disregards defect softening. The second reintroduces defect softening.

Let Φ_0 represent the absolute potential minimum given by Eq. (2.7) above and let $\Delta > 0$ be the energy necessary to create a (noninteracting) vacancy, split-interstitial pair in the system. It is obvious that the presence of one defect in the crystal excludes another from occupying several sites near its position; we will suppose that each inserted vacancy, split-interstitial pair consumes a sites. Assuming that once their positions are fixed each pair can have n distinct configurations, the partition function will be (V = volume, $\beta = 1/k_B T$):

$$Z_N = \exp(-\beta\Phi_0) V Z_{\text{vib}}^{(0)} \sum_{l=0}^{N/A} [n^l \exp(-l\beta\Delta)/(l!)^2] \prod_{k=1}^{l} [N - (k-1)a]^2. \tag{6.3}$$

Here l stands for the number of defect pairs in the system. The last set of factors, indexed by k, enumerates the ways that defect pairs can be sequentially sited within the system. The vibrational partition function has been denoted by $Z_{\text{vib}}^{(0)}$, and in the classical harmonic approximation it will have a product form over independent normal modes

$$Z_{\text{vib}}^{(0)} = \prod_j [\beta\omega_j^{(0)}]^{-1} \tag{6.4}$$

Because we disregard defect softening for the moment, it is consistent to assume that the product of angular frequencies $\omega_j^{(0)}$ is unaffected by the presence of defects.

In the large system limit $\ln Z_N$ will be dominated by the maximum term in the l sum in Eq. (6.3), $l_{\max}$. This is easy to locate by the standard procedure which leads to the expression

$$a l_{\max}/N = a n^{1/2} \exp(-\tfrac{1}{2}\beta\Delta)/[1 + a n^{1/2} \exp(-\tfrac{1}{2}\beta\Delta)] \tag{6.5}$$

The implication is that $l_{\max}$ vanishes at absolute zero and rises smoothly (without a singularity) as temperature rises. In the high temperature limit the system is predicted to contain defects in amount:

$$\lim_{\beta\to 0} l_{\max} = N n^{1/2}/(1 + a n^{1/2}). \tag{6.6}$$

This first stage of description is unacceptable because it fails to yield a melting transition at which $l_{\max}$ is singular. Defect softening eliminates this failure. The form of the partition function modified to take this phenomenon into account is the following:

$$Z_N = \exp(-\beta\Phi_0) V Z_{\text{vib}}^{0} \sum_{l=0}^{N/a} [n^l/(l!)^2] \times \exp[-l\beta\Delta + l^2(\eta + \beta\epsilon)/(2N)] \times \prod_{k=1}^{l} [N - (k-1)a]^2. \tag{6.7}$$

The parameter η measures the effect of defect softening on the normal-mode spectrum, while ϵ represents the strength of a mean-field attraction between defects. Notice that both of these are assumed to be quadratic in l.

The maximum term for Eq. (6.7) in the large system limit is a real positive root of the transcendental equation

$$(a l_{\max}/N)/[1 - (a l_{\max}/N)] = a n^{1/2} \exp\{-\tfrac{1}{2}\beta\Delta + \tfrac{1}{2}(a l_{\max}/N)(\eta + \beta\epsilon)/a\}. \tag{6.8}$$

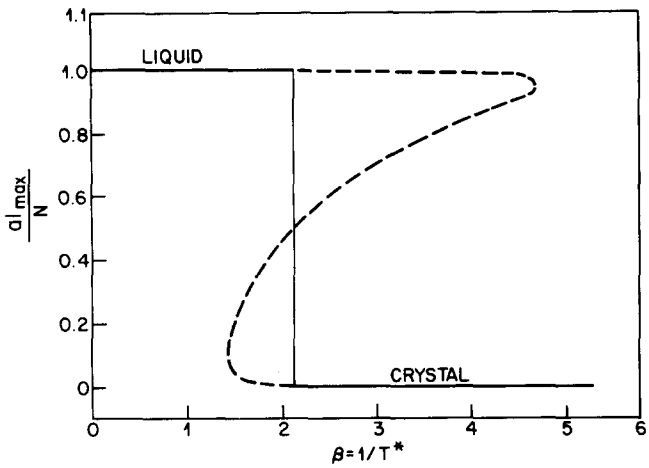

FIG. 14. Defect concentrations obtained from Eq. (6.8). Solid lines correspond to stable equilibrium values, dotted lines to metastable and unstable branches.

To see that this modified version can yield a discontinuous l_{max} as a function of temperature, we have carried out a numerical calculation for the following choice of parameters:

$$\Delta = 10,\ \eta = 200,\ \mathrm{n} = 6,\ \epsilon = 160,\ \mathrm{a} = 20. \tag{6.9}$$

The first of these Δ is the excitation energy discussed in Sec. III. The choice for n considers the possible orientations for a split interstitial. The a value seems to be roughly correct considering the closest approach of defects illustrated in Fig. 8. Finally, η and ϵ were selected to accommodate the data shown in Fig. 13.

A very simple calculation for the parameter set (6.9) yields l_{max} results shown in Fig. 14. The upper and lower branches are analytically connected by a portion that locates "l_{min}", a physically irrelevant solution to Eq. (6.8) that corresponds to a local free energy minimum. The physically relevant l_{max} undergoes a jump discontinuity at

$$T_m^* = 1/\beta_m = 0.469. \tag{6.10}$$

This melting point agrees reasonably well with the observed value 0.43 [Eq. (2.8)]. The upper and lower endpoints of the discontinuity are found to be

$$\begin{aligned} al_{max}/N &= 0.001\ 17 \quad (T^* = /T_m^* - 0), \\ &= 0.998\ 82 \quad (T^* = T_m^* + 0), \end{aligned} \tag{6.11}$$

which indicate, respectively, that coexisting solid and liquid are close to defect free and almost maximally defective.

The approximate method just employed for enumerating defect configurations can be used to estimate the total number Ω of potential energy minima available to the system. This simply requires calculating the packing configuration entropy in the high temperature limit. For large N it is found that asymptotically

$$\Omega \sim N!\exp(0.3912N). \tag{6.12}$$

VII. CONCLUSIONS

The classical many-body system investigated here and in the preceding paper has the bcc crystal as its lowest-potential-energy structure. Molecular dynamics simulation coupled with frequent configuration mapping onto local potential minima reveals that the elementary structural excitations are vacancy, split-interstitial pairs. The system exhibits a defect-softening phenomenon, or mean attraction between defects, which influences the spectrum of normal mode frequencies at the local minima. A simple melting theory incorporating these ideas was constructed which shows that the defect softening is basic to the fact that the solid–liquid phase transition is thermodynamically first order.

In the future it will be desirable to apply the approach followed here to models with other interactions. Also, constant-pressure rather than constant-volume conditions should be explored, particularly since they can create an imbalance between vacancy and interstitial concentrations. It will be interesting to see how the concepts used in this paper will have to be generalized or modified to describe materials with solid–solid phase transitions which precede melting, and materials which first melt into liquid-crystalline phases before becoming isotropic liquids at higher temperature.

[1]F. H. Stillinger and T. A. Weber, Phys. Rev. A **25,** 978 (1982).
[2]F. H. Stillinger and T. A. Weber, Phys. Rev. A **28,** 2408 (1983).
[3]T. A. Weber and F. H. Stillinger, J. Chem Phys. **80,** 2742 (1984).
[4]F. H. Stillinger and T. A. Weber, J. Phys. Chem. **87,** 2833 (1983).
[5]T. A. Weber and F. H. Stillinger, J. Chem. Phys. **81,** 5089 (1984).
[6]C. Kittel, *Introduction to Solid State Physics*, 2nd ed. (Wiley, New York, 1956), pp. 40–41.
[7]B. Henderson, *Defects in Crystalline Solids* (Crane, Russak and Co., New York, 1972), pp. 4,6
[8]D. Weaire, M. F. Ashby, J. Logan, and M. J. Weins, Acta Metal. **19,** 779 (1971).
[9]J. K. Mackenzie and N. F. Mott, Proc. Phys. Soc **63,** 411 (1950).
[10]D. Kuhlman-Wilsdorf, Phys. Rev. A **140,** 1599 (1965).
[11]R. M. J. Cotterill, E. J. Jensen, and W. D. Kristensen, Phys. Lett. A **44,** 127 (1973).
[12]D. R. Nelson and B. I. Halperin, Phys. Rev. B **19,** 2457 (1979).